ARMY RESEARCH LABORATORY

Size-Dependent Strengthening of Particle-Reinforced Aluminum Matrix Composites

by Cyril L. Williams

ARL-TR-5530 **May 2011**

NOTICES

Disclaimers

The findings in this report are not to be construed as an official Department of the Army position unless so designated by other authorized documents.

Citation of manufacturer's or trade names does not constitute an official endorsement or approval of the use thereof.

Destroy this report when it is no longer needed. Do not return it to the originator.

Army Research Laboratory
Aberdeen Proving Ground, MD 21005-5066

ARL-TR-5530 **May 2011**

Size-Dependent Strengthening of Particle-Reinforced Aluminum Matrix Composites

Cyril L. Williams
Weapons and Materials Research Directorate, ARL

REPORT DOCUMENTATION PAGE	Form Approved OMB No. 0704-0188

1. REPORT DATE *(DD-MM-YYYY)*	2. REPORT TYPE	3. DATES COVERED (From - To)
May 2011	Final	January 2010–December 2010

4. TITLE AND SUBTITLE
Size-Dependent Strengthening of Particle-Reinforced Aluminum Matrix Composites

5a. CONTRACT NUMBER

5b. GRANT NUMBER

5c. PROGRAM ELEMENT NUMBER

6. AUTHOR(S)
Cyril L. Williams

5d. PROJECT NUMBER
AH80

5e. TASK NUMBER

5f. WORK UNIT NUMBER

7. PERFORMING ORGANIZATION NAME(S) AND ADDRESS(ES)
U.S. Army Research Laboratory
ATTN: RDRL-WMP-B
Aberdeen Proving Ground, MD 21005-5066

8. PERFORMING ORGANIZATION REPORT NUMBER
ARL-TR-5530

9. SPONSORING/MONITORING AGENCY NAME(S) AND ADDRESS(ES)

10. SPONSOR/MONITOR'S ACRONYM(S)

11. SPONSOR/MONITOR'S REPORT NUMBER(S)

12. DISTRIBUTION/AVAILABILITY STATEMENT
Approved for public release; distribution is unlimited.

13. SUPPLEMENTARY NOTES

14. ABSTRACT
The finite-element-based microstructural modeling technique developed by Suh et al. (Suh, Y. S.; Joshi, S. P.; Ramesh, K. T. *Acta. Mater.* **2009**, *57*, 5848) was reviewed and used for studying the different responses between isotropic and anisotropic aluminum matrix with varying particle sizes. The results show that the overall response of the material was identical when the matrix material was changed from isotropic-elastic/plastic aluminum to anisotropic-elastic/isotropic-plastic aluminum, especially for the 5% volume fraction. However, the anisotropic-elastic/isotropic-plastic aluminum exhibited a lower elastic modulus than that of the isotropic-elastic/plastic-aluminum. Also, the flow stresses were lower for anisotropic-elastic/isotropic-plastic aluminum for the 20% volume fraction.

15. SUBJECT TERMS
size dependent, strengthening, failure, dislocation, particle-reinforced

16. SECURITY CLASSIFICATION OF:			17. LIMITATION OF ABSTRACT	18. NUMBER OF PAGES	19a. NAME OF RESPONSIBLE PERSON
a. REPORT	b. ABSTRACT	c. THIS PAGE			Cyril L. Williams
Unclassified	Unclassified	Unclassified	UU	24	19b. TELEPHONE NUMBER (*Include area code*) 410-278-8753

Contents

List of Figures

List of Tables

INTENTIONALLY LEFT BLANK.

1. Introduction

Materials with high elastic modulus that are considered to be non-deformable relative to the constituent matrix material have long been used to enhance the elastic stiffness and yield strength of lightweight structural metals such as aluminum. When used as particle reinforcements, the average size of these materials can be on the order of several microns. For use in conventional metal matrix composites (MMC), relatively large-size particles in the range of 30–50 μm have been exploited in high volume fractions (*f*) greater than 30% to achieve higher strength. However, this can be detrimental to the overall ductility of the resulting material. It has been observed from experiments that for a fixed *f*, the yield strength of MMCs can increase with decreasing particle size (*1*–*3*). This observation raises the prospect of using smaller particles and low volume fractions compared to conventional MMCs in order to achieve high strengths but also retain ductility. A model based on prismatic punching of dislocations around a particle was proposed by Arsenault and Shi (*1*). The model suggests that this particle size-dependence is due to a geometrically necessary dislocation (GND) density in order to accommodate the plastic strain arising from the mismatch in the coefficient of thermal expansion (CTE) (*4*). Qu et al. (*5*) have suggested that the plastic strain gradients that arise during deformation also generate GNDs due to the elastic-plastic mismatch at the particle-matrix interfaces. However, it was pointed out by Xue et al. (*6*) that the contribution of the yield strength appears to be significantly smaller than that due to the CTE mismatch. The importance of these GND arguments is that they introduce a microstructural length-scale in the otherwise length-scale independent plasticity framework that predicts particle size-dependent strengthening.

To fully understand the behavior of MMCs, there are three characteristics of GND density that are important and require special attention. The first characteristic is that the GNDs will not be uniformly distributed throughout matrix in general but will rather be inclined to cluster close to the reinforcing particles. The length-scale inside the material is established using the average distance the GNDs propagate away from the reinforcing particles. Secondly, the GNDs will often be distributed in a non-symmetric or anisotropic pattern around the reinforcing particle, depending on the shape of the reinforcing particle and the anisotropy of the matrix. Third and finally, the spatial distributions of the reinforcing particles that are non-uniform can result in abnormal GND densities due to the inclusions themselves being clustered in regions of the matrix. Although this may seriously affect the overall strength of the composite material, a more serious implication is on the nucleation and growth of different microstructural failure modes (*7, 8*). Suh et al. (*9*) considered only the first of the three characteristics mentioned previously (the length-scale associated with the GND distributions). In their study, they considered only the spherical particles and neglected the spatial distributions of the reinforcing particles by assuming a periodic array of the reinforcing particles in the matrix. Suh et al. (*9*) investigated the size-

dependent micromechanics of failure in MMCs using the classical continuum approach with dislocation-based micromechanics. Their formulation can be easily implemented in elasto-plastic finite-element analysis (FEA). Their basic idea is that the GNDs that emanate from thermal quenching and the resulting CTE mismatch between the constituent materials are responsible for the highly dislocated volume (punched zone) that surrounds the particle. They calculated the additional dislocation density in the punched zone using the size of the punched volume (*10*). They also calculated the size of the punched zone as a function of the particle size and matrix properties (*11*). The punched zone size and its resulting dislocation density are used in the computational model. As the particles and their surrounding punched zones interact with their neighbors through evolving stress-fields, a non-local interaction arises. The computational approach used by Suh et al. (*9*) retains the capability to model regular and irregular particle distributions while accounting for particle size-dependence using the relevant physics. They demonstrated that in the absence of damage, their model predicts particle size-dependent strengthening that is in accordance with experimental results, especially at small strains. The objective of this report is to extend the model developed by Suh et al. (*9*) to probe the response of a unit-cell consisting of an elastically stiff particle (silicon carbide) and its resulting punched zone in an anisotropic-elastic/isotropic-plastic matrix material (aluminum). The interface between the matrix and the particle that captures the overall size dependent strengthening in the composite is assumed to be perfectly bonded, and hence no form of damage is accounted for. Also, it is assumed that the equations developed by Shibata et al. (*11*) based on the Eshelby inclusion theory for calculating the punched zone size are valid for cylindrical inclusions. Findings from the numerical simulations are compared to those ascertained by Suh et al. (*9*) and further discussed.

2. The Micromechanics of Dislocation Punching

The approach taken here is to reproduce the pertinent equations methodically assembled by Suh et al. (*9*) as they relate to the micromechanics of dislocation punching. During thermal quenching, large stresses are developed in the MMC due to thermoelastic mismatch between the particle and the matrix material. If the stresses are larger than the yield strength of the matrix material, then dislocations are punched out into the matrix material to accommodate the deformation, and this also relaxes the stresses developed. According to Ashby's model (*12*), these changes are geometrically necessary and hence the name geometrically necessary dislocations. It is noteworthy to point out the two possible sources of GNDs. First is the primary source, which represents the dislocations that are punched out into the matrix as a result of the CTE mismatch between the particle and matrix material during cooling of the composite to room temperature from the processing temperature. Analytically, the primary sources are treated as if they have redistributed themselves over the entire matrix to form a background dislocation density (*5*, *13*). However, this is not generally the case (*11*), and these GNDs tend to redistribute

themselves over a length scale l_z, and this redistribution is considered reasonable when l_z is equal to or larger than the spacing between the particles, as shown in figure 1a. This discreteness of the GND redistribution must be accounted for in the micromechanics of composites. The plastic mismatch is the second source of GNDs, and it is the result of the deformation-induced plastic strain gradients that arise during plastic deformation. This is due to the matrix deforming plastically when the particles do not. Although this source of strengthening plays a major role at large strains, its contribution at small plastic strains post yield is not likely to be significant. It has been confirmed by Suh et al. (*9*) that the dominant contribution to particle size-dependent strengthening comes from the thermal quenching stress.

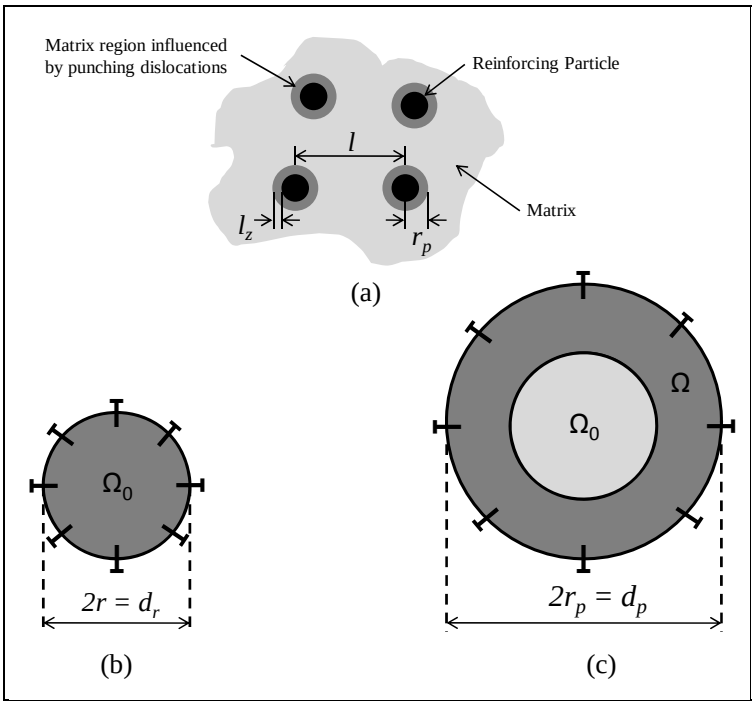

Figure 1. Schematic illustration of (a) discrete distribution of punched regions around individual particles, (b) prismatic punching of dislocations loops due to thermal quenching, and (c) the punched zone boundary corresponding to equilibrium location of punched dislocations (*9*).

Because of the low Zener anisotropy ratio (defined in the next section) of the aluminum matrix, it is reasonable to assume that the excess density due to the GNDs is uniformly distributed in a cylindrical shell called the punched zone of volume (V_z) and size (l_z) bounded by the punched zone size (r_p) and inner particle radius (r). Employing the Ashby model (*12*), the total dislocation line length (L) due to N number of dislocations punched out from a cylindrical particle-matrix interface can be estimated using equation 1:

$$L = 2\pi rN = \frac{8\pi r^2 \varepsilon_p}{b} \approx \frac{k\pi r^2 (\Delta\alpha \Delta T)}{b} \ , \qquad (1)$$

where b is the magnitude of the Burgers vector, $\Delta\alpha = \alpha^* - \alpha$ is the CTE mismatch with α^* being the CTE of the particle and α that of the matrix material, ΔT is the processing temperature change, and ε_p is the plastic strain. The parameter k accounts for the geometry and plastic part of the total thermal strain responsible for the dislocation punching. The excess dislocation density ρ_g in the punched zone can be obtained as follows:

$$\rho_g = \frac{L}{V_z} = \frac{A' r^2 (\Delta\alpha \Delta T)}{b(r_p^3 - r^3)}, \tag{2}$$

where the parameter A' has been determined to be of the order 10^2 (*10*, *12*). Utilizing equation 2 requires the calculation of the punched zone size (r_p), which can be derived from the equations of Shibata et al. (*11*) that are based on the Eshelby inclusion theory. These equations are quite attractive because they account for the effect of other particles (essentially the volume fraction) on the punching distance. Noting that the Eshelby tensor for an elliptic inclusion can be reduced to the Eshelby tensor for a cylindrical inclusion by letting the third dimension approach infinity (*14*), it is assumed that the equations developed by Shibata et al. (*11*) are valid for estimating the punching distance (r_p) from the center of a cylindrical particle. Therefore, r_p is estimated to be

$$r_p = r\left\{\frac{B(1-2Pf) + \sqrt{B^2(1-2Pf)^2 + 16\left(\frac{\tau_y}{G}\right)PB}}{\left(\frac{4\tau_y}{G}\right)}\right\}^{1/3}, \tag{3}$$

for which r is the particle radius and f is the volume fraction of the particles. The coefficients are determined from the following equations as

$$B = \frac{(1+\nu)|\Delta\alpha\Delta T|}{(1-\nu)} \tag{4}$$

and

$$P = \frac{2(1-2\nu)(3\bar{\lambda}+2\bar{G})}{(1-\nu)\left[(1-f)(3\bar{\lambda}+2\bar{G})\frac{(1+\nu)}{(1-\nu)} + 3\{f(3\lambda^*+2G^*) + (1-f)(3\lambda+2G)\}\right]}, \tag{5}$$

where the asterisked material quantities represent those for the particle, and the ones without asterisks represent those for the matrix. Referencing the previous equations, τ is the shear yield strength and ν is the Poisson's ratio of the matrix. Furthermore, $\bar{\lambda} = \lambda^* - \lambda$ and $\bar{G} = G^* - G$ are the mismatches of the Lame constants. Using the approach by Shibata et al. (*11*), it can be deduced that there exists a region around each particle created by the punched zone whose extent is affected by its surrounding particles through the volume fraction f. Therefore, for a given material, smaller volume fractions f (i.e., larger interparticle distances) and larger particle diameters ($d_r = 2r$) could result in punching distances (r_p) large enough to occupy the entire matrix region of the unit-cell or causing the neighboring punched regions to overlap. As in the case with Suh et al. (*9*), a restriction is placed to allow only those combinations of f and r in which such situations do not arise. Most of the particle sizes considered in this work restrict the model to volume fractions (f) that are ≤20%. Finally, using equation 6 in conjunction with the

excess dislocation density calculated in the punched zone (equation 2), the strength of the material within the punched zone due to GND density can be estimated as follows:

$$\sigma = \sigma_y + aGb\sqrt{\rho_g} \quad , \tag{6}$$

where a = 1.25 for aluminum (*15*).

3. Computational Approach

In contrast to the isotropic aluminum matrix material used by Suh et al. (*9*), the aluminum matrix material considered here is a linear-anisotropic-elastic/isotropic-plastic solid. An anisotropic body is one that at a given point has different values of a material property in different directions in that the material properties are directionally dependent. The constitutive equation describing such behavior can be written in indicial notation form as

$$\sigma_i = C_{ij}\varepsilon_j \quad \text{or} \quad \varepsilon_i = S_{ij}\sigma_j \ , \tag{7}$$

where C_{ij} is the stiffness matrix and S_{ij} is the compliance matrix. For anisotropic systems, the Zener anisotropic ratio (A) is defined as

$$A = \frac{2C_{44}}{C_{11}-C_{12}} \ . \tag{8}$$

It is a measure of the anisotropy of a material. Some metals, such as copper, have a high Zener anisotropy ratio (3.21), whereas others, such as aluminum and tungsten, exhibit values close to 1 (1.22 and 1.00, respectively). It is noteworthy to point out that the closer the value is to 1, the more isotropic the material is. Therefore, for tungsten with a value of 1.00, even single crystals are almost isotropic.

For this study, a regular array of cylindrical, linear-elastic silicon carbide (SiC) particles embedded in a linear-anisotropic-elastic/isotropic-plastic aluminum metal matrix is modeled using a finite-element analysis scheme (*16*). The unit-cell consists of the particle, the punched zone, and the matrix, as shown in figure 2a. The particle size and volume fraction are independently controlled, but the punched zone size is adjusted using equation 3. The matrix-particle interface is modeled as perfectly bonded for simplicity. Roller-boundary conditions are imposed at the base of the unit-cell that is pinned on the bottom left corner, and a uniform displacement is applied in the positive y-direction (010) along the top boundary. The composite true stress ($\bar{\sigma}$) and true strain ($\bar{\varepsilon}$) behavior of the unit-cell is derived from the y-displacement, u_y, and the tensile force F_y generated at the top boundary using the following equations:

$$\bar{\sigma} = \frac{1}{{h_c}^2}\int_0^{h_c} F_y\big|_{y=h_c}\, dx \ , \tag{9}$$

and

$$\bar{\varepsilon} = ln\left(1 + \frac{u_y}{h_c}\right), \tag{10}$$

where h_c is the initial height of the unit-cell.

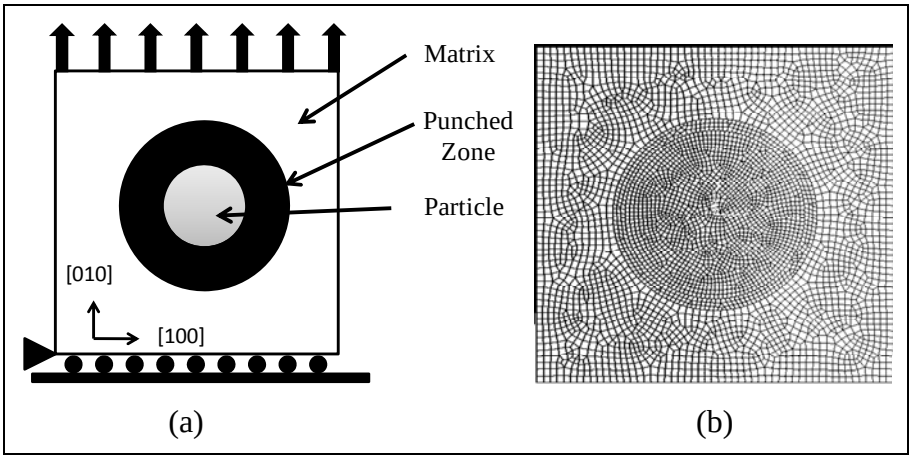

Figure 2. Unit-cell for the case of a perfectly bonded particle-matrix interface.

The meshed unit-cube is shown in figure 2b, and the average number of elements used in a typical simulation is ~17,000 with a concentration of finer mesh in the particle and punched zone region. Prior to the actual simulations, mesh convergence studies were performed to ensure consistent results. The material properties used as input in Abaqus* (*16*) are listed in table 1 (*9*, *17*). The plastic hardening behavior of both the matrix and the punched zone regions was modeled using J_2 flow theory, using as input the uniaxial-stress/plastic-strain relation $\sigma = 464(0.00274 + \varepsilon^p)^{0.136}$ MPa based on experimental data in the open literature (*3*, *5*). The only difference between the plastic-hardening behavior for the matrix and punched zone is that the yield stress for the punched zone is higher than the rest of the matrix material, with the strengthening determined by a thermal quenching ΔT of 474 K (*3*).

Table 1. Material properties for SiC and Al.

Material	**E (GPa)**	**E_{010} (GPa)**	**E_{100} (GPa)**	**ν**	**CTE (1/K)**	**σy (GPa)**	**C_{11} (GPa)**	**C_{12} (GPa)**	**C_{44} (GPa)**
Al	—	63.861	63.861	0.33	23.63×10^{-6}	208	108.2	61.3	28.5
SiC	427	—	—	0.17	4.3×10^{-6}	—	—	—	—

*Abaqus is a registered trademark of Abaqus, Inc.

4. Numerical Results and Discussion

Prior to running FEA simulations, sensitivity studies were conducted with the objective of understanding how the different parameters within the punched zone vary with changes in the particle radius for both volume fractions (5% and 20%, respectively). The results acquired from such studies are shown in figures 3 and 4. From figure 3a, it is observed that increasing the particle radius leads to an increase in punched zone size for both volume fractions, with the largest increase attributed to the 5% volume fraction at a particle radius 16 μm. For both volume fractions, an exponential decay was observed in the dislocation density as the particle size increases and appears to saturate at approximately 16 μm particle radius (figure 3b). It should be noted that prior to saturation, the 5% volume fraction curve is lower than that of the 20%. As a result, the strength of the 20% volume fraction material in the punched zone due to GND is dramatically increased as the particle size is decreased more than that of the 5%. This behavior affects the response of the composite material as shown by Suh et al. (*9*). Similar trends were observed for the yield strength of the punched zone as the particle size was decreased as shown in figure 4c. This implies that as the particle size is decreased, there is a dramatic increase in the yield strength of the punched zone. Finally, when the particle size was increased, the unit-cube size linearly increased in both cases as shown in figure 4d. The unit-cube size with the 5% volume fraction increased at a rate far greater than that of the 20% volume fraction. The physical implication of this is that the particle with the 5% volume fraction is surrounded by a larger matrix than that of the 20% volume fraction.

The response of the composite predicted by Suh et al. (*9*) with varying particle size is shown in figure 5 for both volume fractions. As expected, it was shown by Suh et al. (*9*) that the effect of particle size on the yield strength at 0.2% strain is small at low volume fractions but significant at higher volume fractions. Suh et al. (*9*) were also able to show that for a given volume fraction, the initial work hardening after yield is higher for smaller particle sizes, and this is in good agreement with the experimental observations by Lloyd (*3*). They pointed out that from the continuum viewpoint, this size-dependent strain hardening results from the fractional proportion of the GND zone in the increased unit-cell, which further stiffens the overall plastic response. From figure 4, one can easily notice that for a constant volume fraction, there is a higher overall hardening as the particle size is decreased because smaller particles create stronger punched zones. But from a dislocation mechanics perspective, this behavior may be attributed to the increased forest hardening due to the high dislocation density near the particles. The results for the case where the matrix material was modeled as anisotropic-elastic/isotropic plastic are shown in figures 5 and 6. Figure 5 shows the FEA results for the 20% volume fraction with all three particle sizes (1, 4, and 32 μm). Clearly and intuitively, the regions of high stresses are developed at the interface between the particle and the matrix material due to the mismatch in

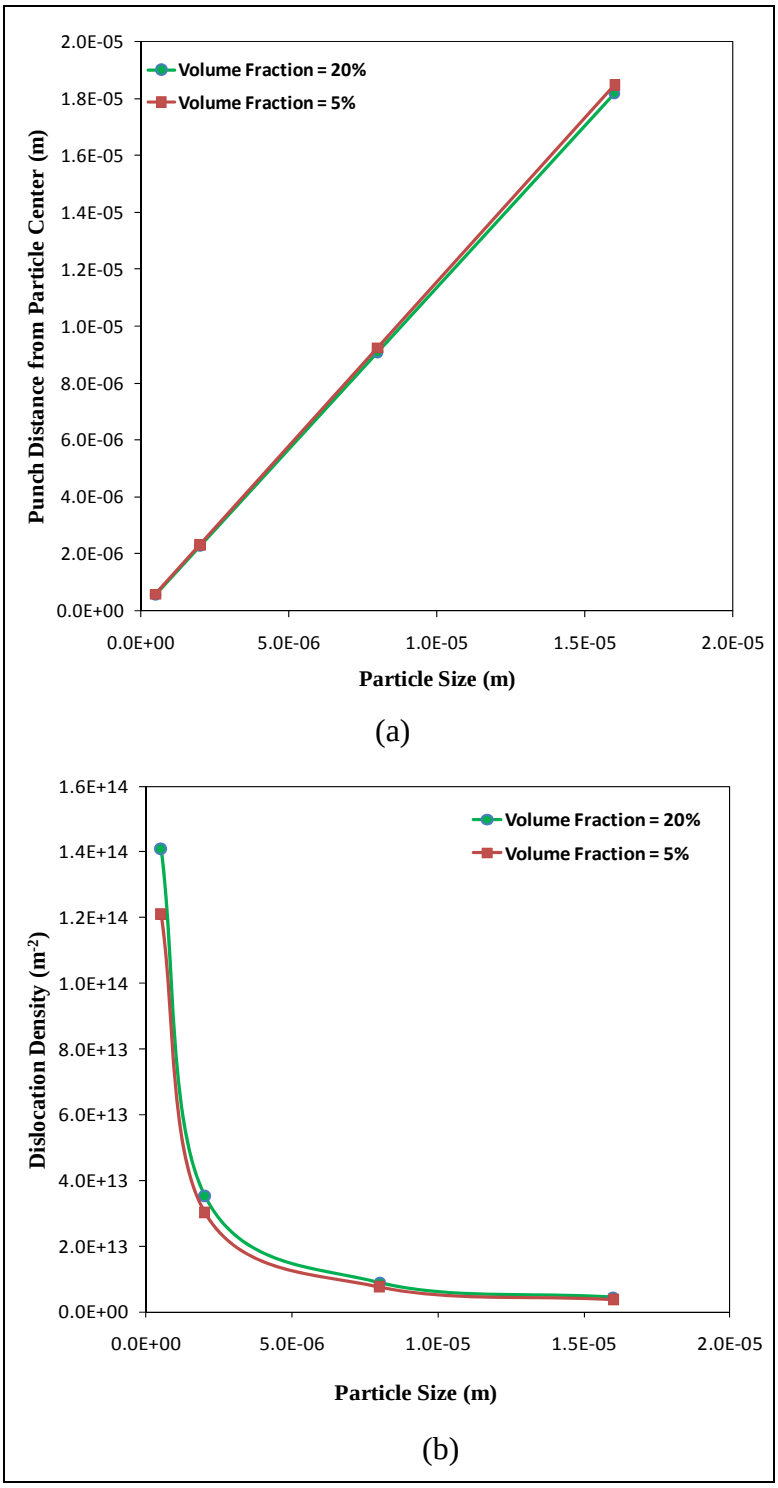

Figure 3. The effects of particle size on punched zone size, dislocation density, yield strength, and unit-cube size for 5% and 20% volume fractions.

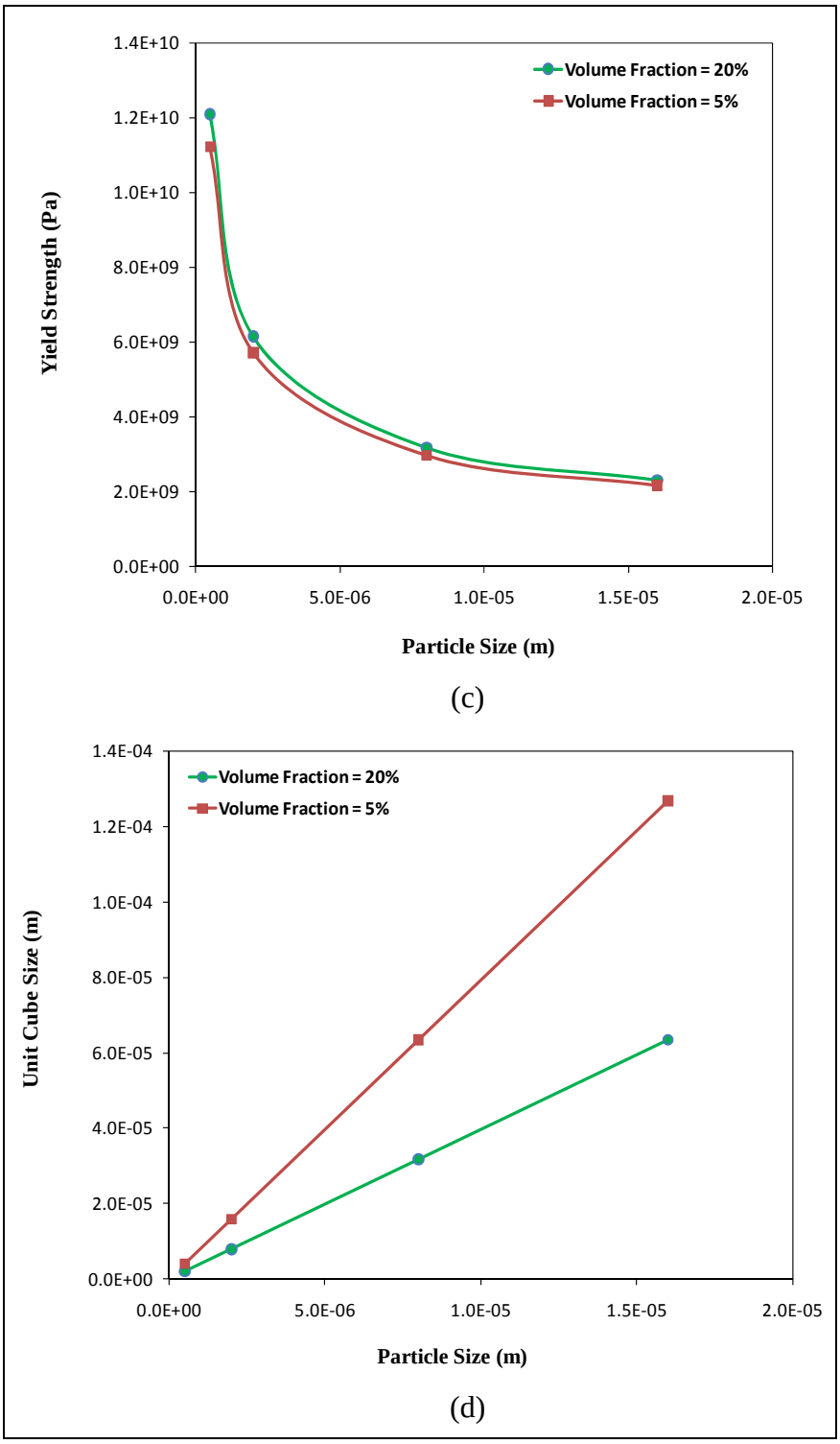

Figure 4. The effects of particle size on punched zone size, dislocation density, yield strength, and unit-cube size for 5% and 20% volume fractions (continued).

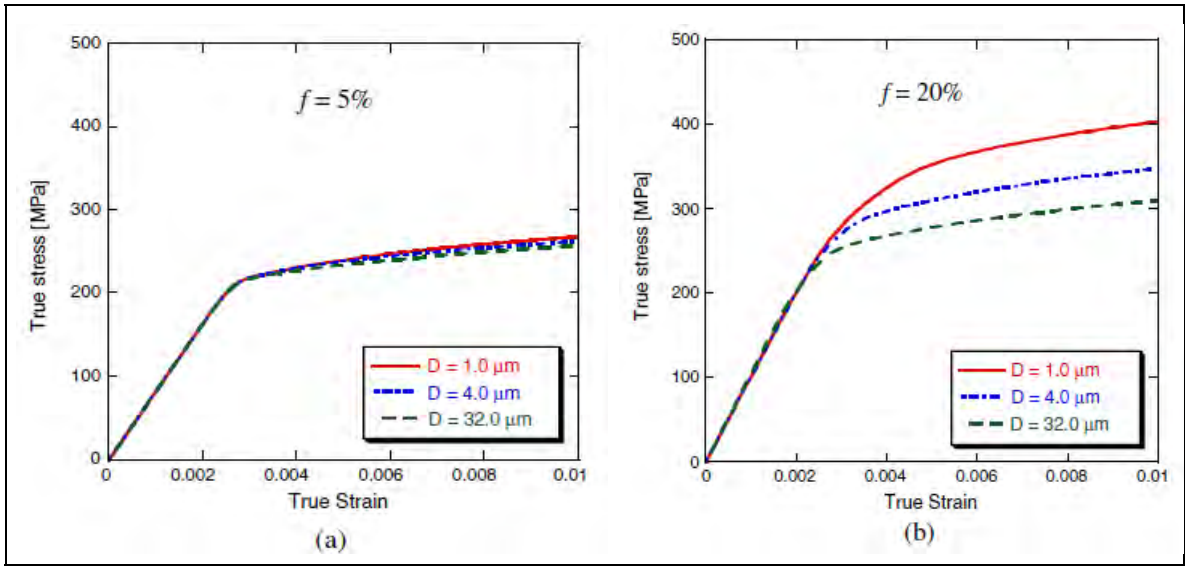

Figure 5. Composite stress-strain curves for (a) f = 5% and (b) f = 20% with different particle sizes (note that the aluminum matrix is isotropic elastic-plastic) (*9*).

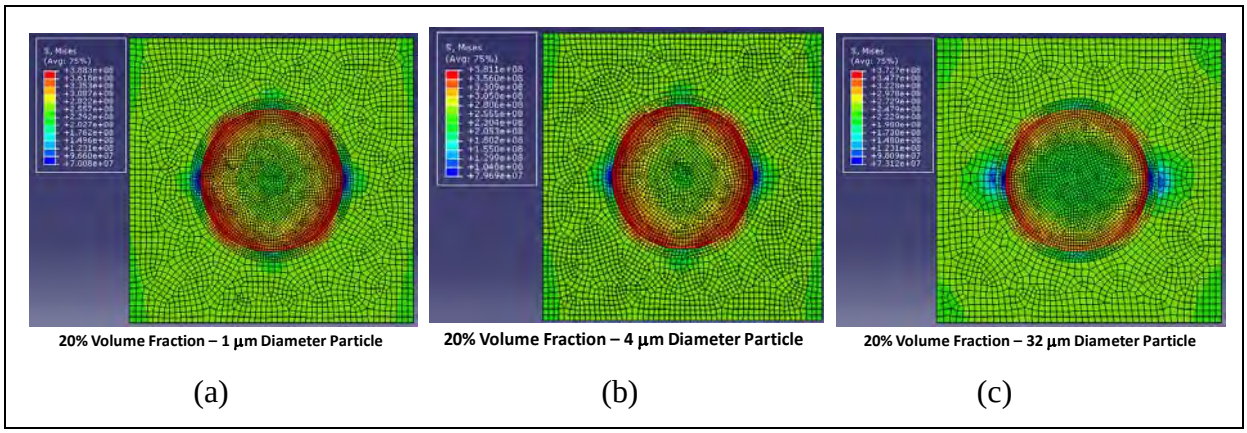

Figure 6. FEA results for the 5% volume fraction with various particle sizes.

yield strength. As shown in figure 6, the overall results in both cases are similar to those obtained by Suh et al. (*9*) except that for the case with anisotropic-elastic/isotropic-plastic matrix material, the elastic modulus was lower in both the (100) and (010) directions (63.861 GPa compared to 76 GPa as in the isotropic elastic-plastic case).

This result was somewhat expected because of the low Zener anisotropic ratio (1.22) approaching full isotropy. Therefore, changing the matrix material from isotropic-elastic/plastic aluminum to anisotropic-elastic/isotropic-plastic aluminum does not produce any gain in yield strength or overall hardening but can lead to substantial reduction in elastic stiffness.

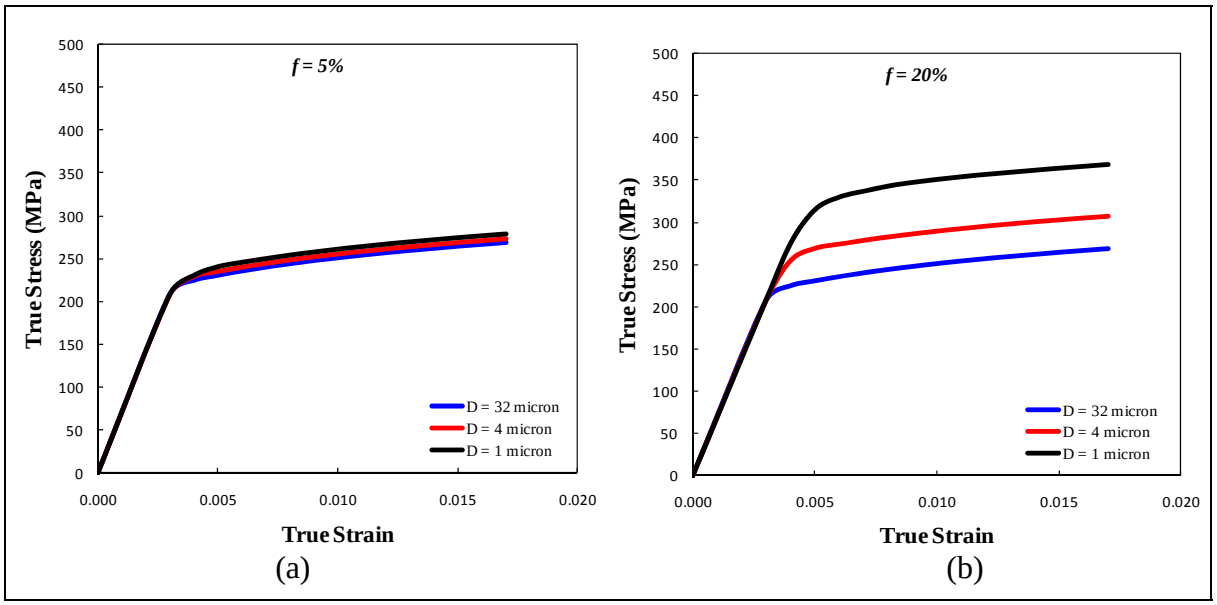

Figure 7. Composite stress-strain curves for (a) f = 5% and (b) 20% with different particle sizes (note that the aluminum matrix is anisotropic elastic-isotropic plastic).

5. Summary

The finite-element-based microstructural modeling technique developed by Suh et al. (*9*) was reviewed and used for studying the different responses between isotropic and anisotropic aluminum matrix with varying particle sizes. The model incorporates a discrete representation of the punched zones in a matrix with excess dislocation density around reinforcing particles due to CTE mismatch, giving a size-dependent composite strengthening. The robustness of this model is that it addresses the size-dependent strengthening using first principles while retaining the simplicity of the conventional unit-cell modeling approach. Furthermore, this model was successfully extended to study the response of a unit-cell with a cylindrical inclusion. The results show that the overall response of the material was identical when the matrix material was changed from isotropic-elastic/plastic aluminum to anisotropic-elastic/isotropic-plastic aluminum, especially for the 5% volume fraction. However, the anisotropic-elastic/isotropic-plastic aluminum exhibited a lower elastic modulus than that of the isotropic-elastic/plastic-aluminum. Also, the flow stresses were lower for anisotropic-elastic/isotropic-plastic aluminum for the 20% volume fraction.

6. References

1. Arsenault, R. J.; Shi, N. *Mater. Sci. Eng.* **1986**, *81*, 175.
2. Ling, Z.; Luo, L.; Dodd, B. *J. Phys. IV: JP* **1994**, 4.
3. Lloyd, D. J. *Int. Mater. Rev.* **1994**, *39*, 1.
4. Dai, L. H.; Ling, Z.; Bai, Y. L. *Compos. Sci. Tech.* **2001**, *61*, 1057.
5. Qu, S.; Siegmund, T.; Huang, Y.; Wu, P. D.; Zhang, F.; Hwang, K. C. *Compos. Sci. Tech.* **2005**, *5*, 1244.
6. Xue, Z.; Huang, Y.; Li, M. *Acta. Mater.* **2002**, *50*, 149.
7. Llorca, J.; Gonzalez, C. *J. Mech. Phys. Solid* **1998**, *46*, 1.
8. Segurado, J.; Llorca, J. *Mech. Mater.* **2006**, *38*, 873.
9. Suh, Y. S.; Joshi, S. P.; Ramesh, K. T. *Acta. Mater.* **2009**, *57*, 5848.
10. Dunand, D. C.; Mortensen, A. *Acta. Metall. Mater.* **1991**, *39*, 127.
11. Shibata, S.; Taya, M.; Mori, T.; Mura, T. *Acta. Metall. Mater.* **1992**, *40*, 3134.
12. Ashby, M. F. *Philos. Mag.* **1970**, *21*, 399.
13. Nan, C. W.; Clarke, D. R. *Acta. Metall. Mater.* **1996**, *44*, 3801.
14. Kim, B. R.; Lee, H. K. *J. Appl. Mech.* **2010**, *77*, 503.
15. Hansen, N. *Acta. Metall.* **1977**, *25*, 863.
16. Abaqus, Inc. Abaqus USER Manual, Version 6.8, 2008.
17. Meyers, M.; Chawla, K. *Mechanical Behavior of Materials*, 2nd ed.; Cambridge University Press: New York, NY, 2009; p 112.

NO. OF COPIES	ORGANIZATION
1 (PDF only)	DEFENSE TECHNICAL INFORMATION CTR DTIC OCA 8725 JOHN J KINGMAN RD STE 0944 FORT BELVOIR VA 22060-6218
1	DIRECTOR US ARMY RESEARCH LAB IMNE ALC HRR 2800 POWDER MILL RD ADELPHI MD 20783-1197
1	DIRECTOR US ARMY RESEARCH LAB RDRL CIM L 2800 POWDER MILL RD ADELPHI MD 20783-1197
1	DIRECTOR US ARMY RESEARCH LAB RDRL CIM P 2800 POWDER MILL RD ADELPHI MD 20783-1197
1	DIRECTOR US ARMY RESEARCH LAB RDRL D 2800 POWDER MILL RD ADELPHI MD 20783-1197
	ABERDEEN PROVING GROUND
1	DIR USARL RDRL CIM G (BLDG 4600)

NO. OF COPIES	ORGANIZATION
1 (CD only)	DPTY ASSIST SCT FOR R&T SARD TT ASA ACT J PARMENTOLA THE PENTAGON RM 3E479 WASHINGTON DC 20310-1714
3	AIR FORCE ARMAMENT LAB AFATL DLJW W COOK D BELK J FOSTER EGLIN AFB FL 32542
2	NSF S MCKNIGHT G PAULINO 4201 WILSON BLVD STE 545 ARLINGTON VA 22230-0002
1	DARPA W COBLENZ 3701 N FAIRFAX DR ARLINGTON VA 22203-1714
1	DIRECTOR US ARMY ARDEC AMSRD AAR AEE W E BAKER BLDG 3022 PICATINNY ARSENAL NJ 07806-5000
2	US ARMY TARDEC AMSTRA TR R MS 263 K BISHNOI D TEMPLETON MS 263 WARREN MI 48397-5000
1	COMMANDER US ARMY RSRCH OFC RDRL ROE N B LAMATTINA PO BOX 12211 RESEARCH TRIANGLE PARK NC 27709-2211
1	COMMANDER US ARMY RSRCH OFC RDRL ROI M J LAVERY PO BOX 12211 RESEARCH TRIANGLE PARK NC 27709-2211

NO. OF COPIES	ORGANIZATION
1	COMMANDER US ARMY RSRCH OFC RDRL ROE M D STEPP PO BOX 12211 RESEARCH TRIANGLE PARK NC 27709-2211
5	NVL RSRCH LAB E R FRANCHI CODE 7100 M H ORR CODE 7120 J A BUCARO CODE 7130 J S PERKINS CODE 7140 S A CHIN BING CODE 7180 4555 OVERLOOK AVE SW WASHINGTON DC 20375
1	ERDC US ARMY CORPS OF ENGINEERS USACEGSL P PAPADOS 7701 TELEGRAPH RD ALEXANDRIA VA 22315
1	AFOSR/NL 875 NORTH RANDOLPH ST STE 325 RM 3112 F FAHROO ARLINGTON VA 22203
5	SOUTHWEST RSRCH INST C ANDERSON K DANNEMANN T HOLMQUIST G JOHNSON J WALKER PO DRAWER 28510 SAN ANTONIO TX 78284
1	COMPUTATIONAL MECH CONSULTANTS J A ZUKAS PO BOX 11314 BALTIMORE MD 21239-0314
1	DTRA M GILTRUD 8725 JOHN J KINGMAN RD FORT BELVOIR VA 22060

NO. OF COPIES ORGANIZATION

1 APPLIED RSCH ASSOCIATES
D E GRADY
4300 SAN MATEO BLVD NE
STE A220
ALBUQUERQUE NM 87110

1 INTERNATIONAL RSRCH ASSOC INC
D L ORPHAL
4450 BLACK AVE
PLEASANTON CA 94566

3 ORNL
ENVIRON SCI DIV
W DOLL
T GAMEY
L BEARD
PO BOX 2008
OAK RIDGE TN 37831

1 NATL INST OF STANDARDS &TECHLGY
BLDG & FIRE RSRCH LAB
J MAIN
100 BUREAU DR MS 8611
GAITHERSBURG MD 20899-8611

2 MATERIALS SCI CORP
A CAIAZZO
R LAVERTY
181 GIBRALTAR RD
HORSHAM PA 19044

1 DIR USARL
RDRL D
V WEISS
2800 POWDER MILL RD
ADELPHI MD 20783-1197

1 DIR USARL
RDRL SE
J PELLEGRINO
2800 POWDER MILL RD
ADELPHI MD 20783-1197

1 DIR USARL
RDRL SES P
A EDELSTEIN
2800 POWDER MILL RD
ADELPHI MD 20783-1197

NO. OF COPIES ORGANIZATION

1 DIR USARL
RDRL DP
M CHOWDHURY
2800 POWDER MILL RD
ADELPHI MD 20783-1197

ABERDEEN PROVING GROUND

112 DIR USARL
RDRL WM
DIRECTOR (A)
T DIGLIANI
B FORCH
S KARNA
J MCCAULEY
P PLOSTINS
RDRL WML
J NEWILL
M ZOLTOSKI
RDRL WML B
I BATYREV
B RICE
N WEINGARTEN
RDRL WML D
P CONROY
M NUSCA
RDRL WML G
M BERMAN
W DRYSDALE
RDRL WML H
T FARRAND
R SUMMERS
M FERMEN-COKER
L MAGNESS
B SORENSEN
E KENNEDY
T EHLERS
C MEYER
D SCHEFFLER
S SCHRAML
B SCHUSTER
RDRL WMM
R DOWDING
J ZABINSKI
RDRL WMM A
M MAHER
J SANDS
J TZENG
E WETZEL
RDRL WMM B
T BOGETTI
B CHEESEMAN
C FOUNTZOULAS
D HOPKINS

NO. OF COPIES ORGANIZATION

B POWERS
C RANDOW
M VANLANDINGHAM
R WILDMAN
C F YEN
RDRL WMM D
E CHIN
K CHO
R HOWELL
RDRL WMM E
M COLE
T JESSEN
J LASALVIA
RDRL WMM F
L KECSKES
E KLEIR
RDRL WML G
J ANDZELM
A RAWLETT
RDRL WMP
P BAKER
S SCHOENFELD
RDRL WMP B
R BECKER
S BILYK
D CASEM
J CLAYTON
M GREENFIELD
C HOPPEL
R KRAFT
B LEAVY
M SCHEIDLER
T WEERASOORIYA
C WILLIAMS (10 CPS)
RDRL WMP C
T BJERKE
S SEGLETES
G BOYCE
R MUDD
N BRUCHEY
W WALTERS
RDRL WMP D
R DONEY
J RUNYEON
B SCOTT
D KLEPONIS
K STOFFEL
RDRL WMP E
M BURKINS
W GOOCH
T JONES
B LOVE (10 CPS)
M LOVE

NO. OF COPIES ORGANIZATION

RDRL WMP F
R BITTING
M CHOWDHURY
E FIORAVANTE
A FRYDMAN
N GNIAZDOWSKI
R GUPTA
RDRL WMP G
N ELDREGE
R EHLERS
W BUKOWSKI
B KRZEWINSKI
S KUKUCK
R BANTON
D KOOKER
G R PEHRSON